Photodissociation of NO2 at 355 and 351 nm Investigated by Photofragment Translational Spectroscopy

ARTICLE *in* THE JOURNAL OF PHYSICAL CHEMISTRY · NOVEMBER 1994

Impact Factor: 2.78 · DOI: 10.1021/j100098a023

Photodissociation of NO_2 at 355 and 351 nm Investigated by Photofragment Translational Spectroscopy

J. A. Harrison,† X. Yang,‡ M. Rösslein, P. Felder, and J. Robert Huber*

Physikalisch-Chemisches Institut der Universität Zürich, Winterthurerstrasse 190, CH-8057 Zürich, Switzerland

Received: May 19, 1994; In Final Form: September 20, 1994®

The photodissociation of jet-cooled NO_2 at 355 and 351 nm has been investigated by polarized high-resolution photofragment translational spectroscopy. The translational energy distributions $P(E_T)$ of the nascent photofragment pairs NO + O were derived from the measured time-of-flight (TOF) distributions. By comparison of $P(E_T)$ with the available energy, the population of vibrationally excited NO was determined to be $P(v=0) = 62 \pm 3\%$ and $P(v=1) = 38 \mp 3\%$ at 355 nm and $P(v=0) = 57 \pm 3\%$ and $P(v=1) = 43 \mp 3\%$ at 351 nm. These findings are consistent with the trend predicted by statistical models of the dissociation process. Nonstatistical decay dynamics are, however, indicated for the rotational degrees of freedom as manifested by bimodal (or multimodal) rotational distributions of NO(v=0,1). The recoil anisotropy parameter β as a function of fragment translational energy was obtained from the polarized TOF spectra and was found to depend on the photolysis wavelength and on the vibrational state of the NO product: $\beta(v=0) = 1.42$ and $\beta(v=1) = 1.25$ at 355 nm, whereas $\beta(v=0) = 1.77$ and $\beta(v=1) = 1.48$ at 351 nm. The NO rotational alignment $A_0^{(2)}$ measured by the laser-induced fluorescence method is at high J values close to the theoretical (perpendicular-type) limit of −0.4 at both photolysis wavelengths. This result, in conjunction with the values of β, implies that the photon absorption occurs via the $^2B_2 \leftarrow {}^2A_1$ electronic transition and that the photodissociation takes place essentially without anisotropy loss and hence on a subpicosecond time scale. The observed dependence of β on the product vibrational state suggests two different decay pathways with quantum mechanical effects playing an important role.

1. Introduction

The spectroscopy and photodissociation of nitrogen dioxide NO_2 have been and still remain of interest, in particular as a topic which greatly contributes to our understanding of the interplay between structure and dynamics in a molecular system.[1] The visible absorption spectrum of this simple triatomic molecule is highly complex due to extensive interstate coupling, the effect of which is also manifested in the electronic relaxation and the photochemical decay. With excitation close to the dissociation threshold energy ($D_0 = 25\,130 \pm 2$ cm^{-1} [2,3]), the latter process leads to the products NO($X^2\Pi_{\Omega=1/2,3/2}$) and O($^3P_{J=2,1,0}$) both in their electronic ground states and exhibits interesting features of a statistical as well as a nonstatistical nature. For a review of experimental and theoretical results pertinent to the present photodissociation work, the reader is referred to the Introduction of the recent articles by Reisler and co-workers[3,4] and by Wittig and co-workers.[5]

In their pioneering work on photofragment translational spectroscopy, Busch and Wilson[6] investigated NO_2 in an effusive beam to demonstrate the time-of-flight (TOF) crossed laser molecular beam method. With laser excitation at 347 nm (28 810 cm^{-1}), and at a fixed scattering angle of 90°, they measured the center-of-mass kinetic energy[6] and angular distribution[7] of the fragments. These results were later analyzed by Quack and Troe,[8] who applied the statistical adiabatic channel model. Although the fitting of the theoretical and experimental data was not perfect, they concluded—opposite to the original interpretation of Busch and Wilson—that the measured kinetic energy release is consistent with a statistical distribution. However, a few years later Welge and co-workers[9,10] inferred a nonstatistical decay process. They reinvestigated the NO_2 photodissociation in the bulk phase and in a cold beam at λ_{exc} = 351, 337, and 308 nm using the laser-induced fluorescence (LIF) detection technique to probe the rotational, vibrational, and electronic (fine-structure states) distributions of the NO fragments.[2] Neither the vibrational nor the rotational nor the spin state distributions were found to be consistent with a statistical decay model.

From the numerous spectroscopic and photochemical studies that followed we restrict ourselves to the most recent ones. The imaging technique of state-selected photofragments from the photolysis of NO_2 at 355 nm in a supersonic beam was used by Suzuki *et al.*[11] to determine the photofragment velocity distribution and recoil anisotropy parameter β. In contrast to previous measurements ($\beta = 0.74$ at 347 nm[7] and $\beta = 0.9$ at 360 nm[12]), these workers found $\beta = 1.2 \pm 0.3$ and explained the discrepancy as due to the effect of the rotation of the parent molecule. Similar values were determined by Butenhoff and Rohlfing,[13] who applied photofragment transient gratings to determine β of state-selected and extremely slow-moving NO fragments produced upon excitation only 126 cm^{-1} above the dissociation threshold. Pfab and co-workers[14] studied the photolysis of jet-cooled NO_2 at 355 nm by probing the nascent product NO(v=1) with one-photon LIF. They found a bimodal rotational distribution and a pronounced rotational alignment ($A_0^{(2)} = -0.35 \pm 0.05$).

Ionov *et al.*[5,15] measured the unimolecular decomposition rate $k(E)$ of expansion cooled NO_2 after excitation with tunable subpicosecond laser pulses of 375−402 nm and monitored the time evolution of the NO product LIF. From the decomposition threshold at 25 130 cm^{-1} to an energy of 26 126 cm^{-1}, $k(E)$ was found to increase from 1.6×10^{11} to 2.8×10^{12} s^{-1} in a somewhat steplike fashion. This latter effect, which is absent

† Present address: Department of Chemistry, Massey University, Private Bag 11-222 Palmerston North, New Zealand.

‡ Present address: P.O. Box 100, Dalian 116012, People's Republic of China.

® Abstract published in *Advance ACS Abstracts,* November 1, 1994.

0022-3654/94/2098-12260$04.50/0

in room temperature samples where a smooth variation of $k(E)$ is observed, was suggested to reflect the sequential opening of bending modes of the transition state. These experimental findings were discussed in a theoretical analysis by Klippenstein and Radivoyevitch.[16]

Parallel to a study of Miyawaki *et* al.,[17] Reisler and coworkers[3,4] addressed in two recent LIF studies the NO product state distribution of jet-cooled NO_2 using excitation from the dissociation threshold up to an excess energy of 3000 cm^{-1}. The rotational state distributions were found to be consistent with the result from phase space theory and hence with a loose activated complex, while the vibrational population followed closely the prediction of variational RRKM theory. This good agreement with statistical theory was taken as evidence for a vibrational predissociation mechanism that involves strongly mixed vibronic levels of predominantly ground state character. Furthermore, extensive photofragment yield measurements revealed distinct fluctuation patterns in the rotational distribution of each vibrational NO state. This result, together with their findings on the vibrational and electronic (fine-structure) level distributions, led the authors to suggest a hierarchy of adiabaticity for the different degrees of freedom: the NO vibrational states first become adiabatic followed by the rotational and finally the electronic degrees of freedom.[3]

The present work reports on a reinvestigation of the photodissociation of NO_2 by photofragment translational spectroscopy[18-20] with variable scattering angle. Using excitation wavelengths of 355 and 351 nm, we measured the TOF spectra and hence the kinetic energy distribution of the photofragments O and NO and their spatial distribution ($\vec{\mu}-\vec{v}$ correlation) in order to determine the disputed vibrational energy distribution in NO as well as the anisotropy parameter β and its dependence on the translational energy or vibrational state. The polarization data were supplemented by LIF measurements of the rotational alignment $A_0^{(2)}$ ($\vec{\mu}-\vec{J}$ correlation). The study demonstrates and illustrates by means of a prototypical photochemical decay the potential of polarized high-resolution photofragment translational spectroscopy.

2. Experiment

A description of our high-resolution photofragment translational spectrometer has been given elsewhere.[21] A pulsed molecular beam of NO_2 seeded in helium was generated with a specially designed corrosion resistant valve driven by a piezoelectric translator.[22] NO_2 was synthesized by the reaction of NO with oxygen, and the resulting sample was purified by several freeze−pump−thaw cycles until the frozen compound was white. A gas mixture of 0.4% was then prepared by flowing He carrier gas with a stagnation pressure of 600 mbar through a distilled liquid sample of NO_2 cooled to −53 °C. It was necessary to leave the source pulsing for several hours in order to obtain stable molecular beam conditions. The velocity distribution $f(v) = C \exp[-(v - v_0)^2/\alpha^2]$ of the beam was determined by the laser-induced hole burning method[23] which yielded typical values of $v_0 = 1600$ m/s and $\alpha = 80$ m/s, corresponding to a speed ratio of 20.

The photolysis at 351 nm was performed with a XeF excimer laser (Lambda Physik EMG101 MSC) which was mildly focused at the intersection with the molecular beam. In addition to its main emission band at 351 nm, this laser radiates also at 349 and 353 nm, with the latter two band systems contributing each ~20% to the total laser intensity. At the highest pulse energy of 50 mJ, about 12% of the irradiated NO_2 molecules are photolyzed. TOF measurements with the unpolarized laser were carried out at several laboratory scattering angles Θ (where Θ is the angle between the molecular beam and the detector axis) to ensure optimal kinematic conditions for the photofragment detection. Since, at small angles ($\Theta < 18°$), a signal from undissociated NO_2 effusing from the source chamber is observed at long flight times, the TOF spectra were obtained as the difference signals recorded with the photolysis laser firing only every second pulse of the molecular beam source. For the determination of the photofragment recoil anisotropy the laser was linearly polarized with a stack of Brewster plates followed by a rotatable half-wave plate. The degree of polarization of the laser, defined here as the intensity of the desired polarization divided by the total laser intenity, was carefully determined at the intersection with the molecular beam by means of a quartz plate oriented at Brewster's angle. The reflected light intensity was measured with a power meter (Scientech 362) as a function of the angular setting of the half-wave plate, from which a degree of polarization of 93 ± 1% was obtained. The angular distribution of the photofragments was determined by recording the TOF signal at fixed angle Θ as a function of the polarization angle ϵ, which is the angle between the electric vector and the detection axis. For simplicity, we shall henceforth use the terms "polarized TOF data" and "unpolarized TOF data".

Photolysis at 355 nm was carried out with the third harmonic of a Nd:YAG laser (Continuum POWERLITE 7020). The spectral bandwidth at 355 nm is specified to be <2 cm^{-1}. The unfocused output was collimated with a pair of apertures providing a beam with a diameter of 3 mm and a pulse energy of 50 mJ. Since this laser is linearly polarized (>99%), the unpolarized TOF spectra were obtained by summation of the polarized data recorded with mutually orthogonal polarizations.

The photofragment TOF distributions were measured both at $m/e = 30$ (NO^+) and $m/e = 16$ (O^+). While most of the data were taken at $m/e = 30$ where the signal-to-noise ratio is particularly good, measurements were also performed for $m/e = 16$ in order to test the consistency of the derived recoil distributions. It is noted that all the TOF distributions shown in the following section have been corrected for the transit time of the ions through the mass filter.

The dimeric form N_2O_4 is a potential source of artifacts in the TOF distributions. First, its primary dissociation product NO_2 is readily fragmented to NO^+ in the detector and will thus contribute to the TOF signal at $m/e = 30$. Second, the NO_2 formed upon the photolysis of N_2O_4 can absorb a further photon and thereby produce secondary NO fragments. For this reason, careful tests were conducted to establish the effect of N_2O_4 which, while being negligible under the conditions prevailing in the room temperature beam source, can be formed in the ensuing supersonic expansion.

In addition to the PTS measurements, the nascent NO fragments were also probed by LIF spectroscopy to determine the rotational alignment parameter $A_0^{(2)}$. The experimental setup and the method have been described in full details elsewhere.[24,25] The photolysis and probe laser pulses were generated with two dye lasers pumped by the same excimer laser. The photolysis laser was operated at <2 mJ/pulse (line width ~ 0.7 cm^{-1}) while the probe laser (line width ~ 0.3 cm^{-1}) was operated at <1 mJ/pulse to avoid saturation of the NO excitation. The counterpropagating laser beams were crossed in the vacuum chamber at an angle of ~1.5°, with the intersection being located 15 mm (30 nozzle diameters) below the orifice of the pulse valve. Both lasers were linearly polarized with a degree of polarization ≥98%, and the plane of polarization of the dissociation laser was rotated by Fresnel rhombs. The NO fragment was probed by 2 + 1 LIF using an unpolarized

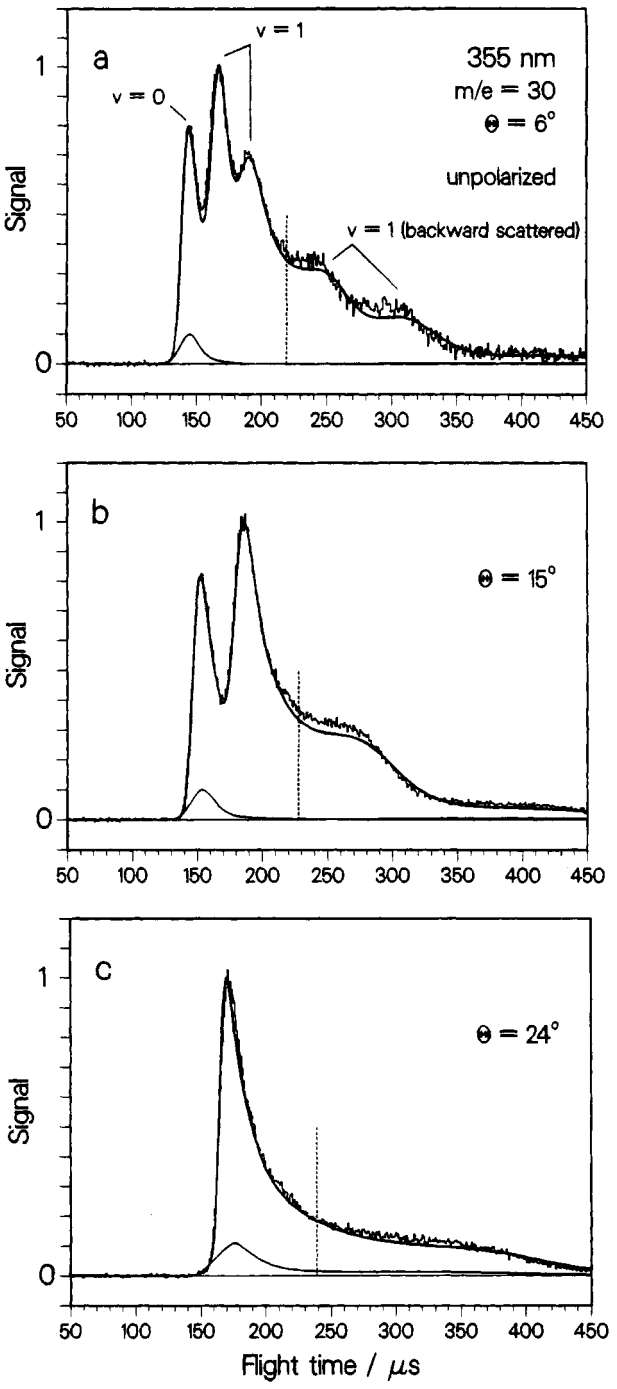

Figure 1. Photodissociation of NO_2 at 355 nm. Unpolarized TOF distributions of the NO fragment (m/e = 30) measured at the LAB angles Θ = 6° (a), 15° (b), and 24° (c). The thick solid lines are the best-fitting TOF distributions calculated with the $P(E_T)$ given in Figure 4a. The thin solid line represents the small contribution from NO_2 produced in the photolysis of N_2O_4. The dashed vertical line denotes the separation between forward and backward scattered photofragments.

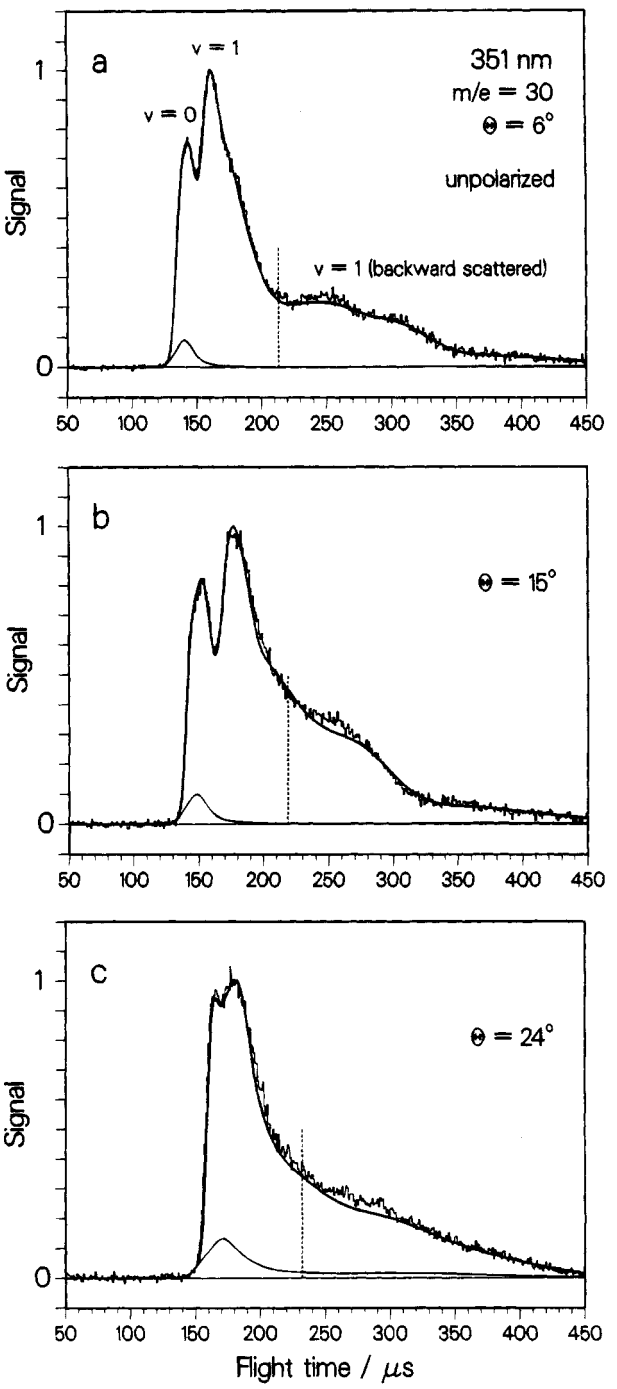

Figure 2. Photodissociation of NO_2 at 351 nm. Unpolarized TOF distributions of the NO fragment (m/e = 30) measured at the LAB angles Θ = 6° (a), 15° (b), and 24° (c). The thick solid lines are the best-fitting TOF distributions calculated with the $P(E_T)$ given in Figure 4b. The thin solid line represents the small contribution from NO_2 produced in the photolysis of N_2O_4. The dashed vertical line denotes the separation between forward and backward scattered photofragments.

detector which was positioned at right angles to the plane formed by the laser beams.

3. Results and Analysis

3.1. PTS Experiments. The unpolarized TOF distributions of the NO fragments (m/e = 30) formed upon NO_2 photolysis at 355 and 351 nm, measured with scattering angles Θ = 6°, 15°, and 24°, are displayed in Figures 1 and 2, respectively. The TOF signals of the O atoms (m/e = 16) are shown in Figure 3. The solid lines given in Figures 1–3 are the calculated best-fitting distributions which were obtained as follows. The TOF data were first analyzed with a new and direct deconvolution method that will be described in detail in a future publication.[26] In brief, an optimal filter is applied to remove the shot noise from the TOF data. Subsequently, the experimental broadening due to the finite width of the ionizer and finite laser photolysis region is deconvoluted from the TOF distribution by means of a Fourier transform method. After transformation from the laboratory (LAB) to the center-of-mass (CM) frame and deconvolution of the contributions from the angular spread and translational temperature of the molecular beam, one obtains the total translational energy distribution $P(E_T)$. Since the $P(E_T)$ curves derived from individual TOF spectra inevitably show

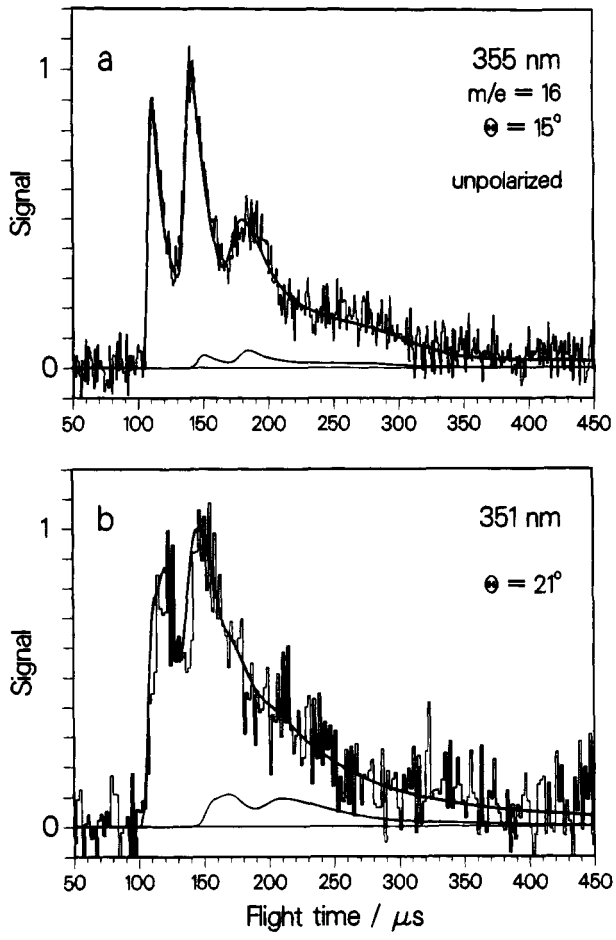

Figure 3. Photodissociation of NO_2. Unpolarized TOF distributions of the O atom (m/e = 16) measured at 355 nm (a) and 351 nm (b). The thick solid lines are the best-fitting TOF distributions calculated with the $P(E_T)$ given in Figure 4, and the thin solid lines represent the small contribution from NO cracked to O^+ in the ionizer.

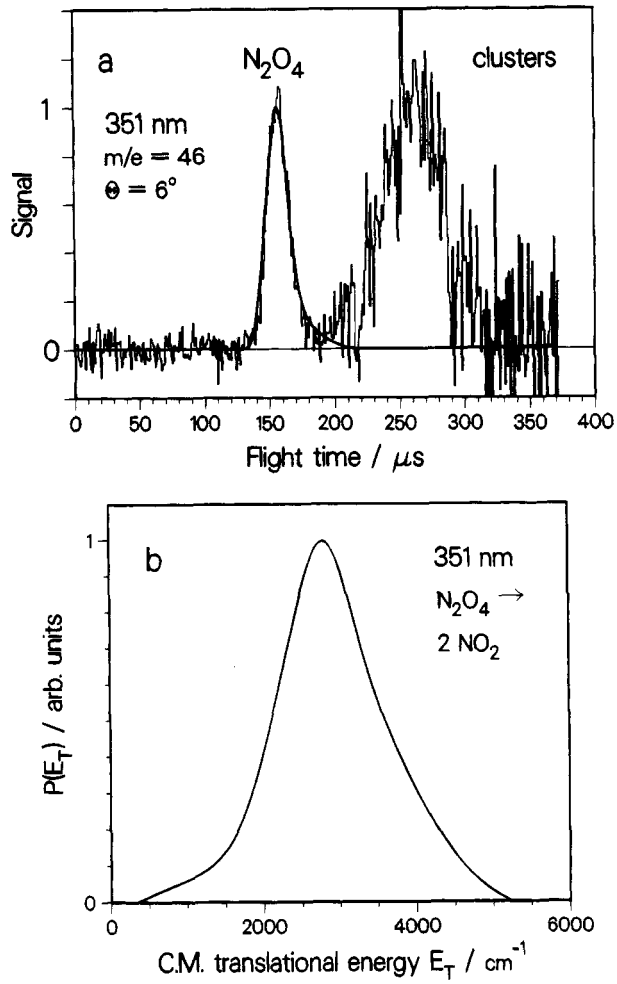

Figure 4. Photodissociation of N_2O_4 at 351 nm: (a) unpolarized TOF distribution of the NO_2 fragment (m/e = 46) measured at Θ = 6° with a beam containing 8.5% NO_2; (b) total translational energy distribution of the photofragment pairs.

slight deviations among each other, a "compromise" or global $P(E_T)$ must be deduced. In a second step of the analysis, the $P(E_T)$ was iteratively refined with the conventional forward convolution technique.[27,28] This additional step was necessary in order to take into account the photodissociation of N_2O_4 which contributes to the signal in the early part of the TOF spectrum.

The translational energy release in the photolysis of N_2O_4 was studied by measuring the TOF signal of the NO_2 product at m/e = 46. The result is shown in Figure 4a for the case of 351 nm excitation, along with the corresponding $P(E_T)$ distribution which is given in Figure 4b. The data were obtained with a beam containing 8.5% NO_2 in order to enhance formation of N_2O_4. Under these conditions there is also substantial formation of $(NO_2)_n$ clusters, the photolysis of which produces the broad TOF peak near 270 μs. This feature disappears at lower NO_2 concentration, and hence, the photodissociation of $(NO_2)_n$ does not contribute to the signals recorded with the diluted (0.4%) NO_2 beam. With the $P(E_T)$ given in Figure 4b the shape of the TOF signal at m/e = 30, caused by fragmentation of NO_2 to NO^+ in the ionizer, can be calculated for arbitrary scattering angles. The relative importance of the contribution from N_2O_4 photolysis was then established in three independent ways. First, the absolute TOF signal (in counts/laser shot) measured at m/e = 46 was rescaled according to the relative intensity of NO^+ and NO_2^+ in the mass spectrum of NO_2, which in turn was determined in a separate experiment. Second, a comparison was made of the TOF signals at m/e = 30 obtained with various concentrations of NO_2 and a constant total stagnation pressure. Since the photolysis of N_2O_4 contributes only to the first TOF peak at m/e = 30, the intensity ratio of the first and second TOF peak plotted as a function of NO_2 concentration and extrapolated to the case of infinite dilution yielded the intensity ratio expected in the absence of N_2O_4. Third, the TOF distributions of the O atoms shown in Figure 3 were included in the analysis. Since the signal at m/e = 16 is virtually unaffected by the photolysis of N_2O_4, the adequacy of the $P(E_T)$ distribution can be tested by comparing the predicted TOF spectrum of the O atoms with the experimental data.

The $P(E_T)$ distributions that provide the best fits of the unpolarized data are displayed in Figure 5. The fact that these $P(E_T)$ can also reproduce the undulations observed at long flight times due to photofragments ejected in the *backward* direction with respect to the molecular beam represents a stringent test of our kinematic simulations. Obviously, the photofragment signal at kinetic energies above the threshold for the formation of vibrationally excited NO is unambiguously attributed to O + NO(v=0). Moreover, the sharp signal rise near the energy threshold for the formation of vibrationally excited NO, shown by the arrows in Figure 5, leads us to conclude that *most of the signal at a kinetic energy below that threshold is due to the formation of O + NO(v=1).* However, before further discussing the vibrational distribution of NO, a small correction must be applied to the "unpolarized" $P(E_T)$ distributions in order to account for the recoil anisotropy not being constant over the whole translational energy range.

The angular distribution of the photofragments is given by $w(\theta) = (4\pi)^{-1}[1 + \beta P_2(\cos\theta)]$, where θ denotes the angle

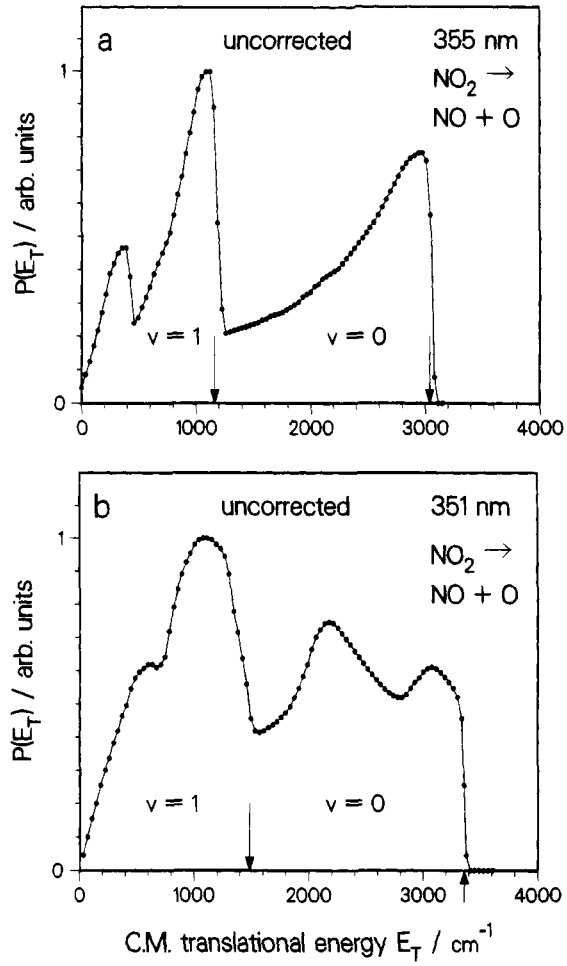

Figure 5. Total translational energy distributions of the fragment pairs produced in the photolysis of NO_2 at 355 nm (a) and 351 nm (b). The vertical arrows indicate the energy thresholds for the formation of NO in the two lowest vibrational states (see Table 1). These $P(E_T)$ are the best-fitting distributions of the unpolarized TOF data and have not been corrected for the energy-dependent recoil anisotropy (see text).

between the electric vector $\vec{E}$ of the laser and the recoil velocity $\vec{v}$ in the CM system, and β is the so-called anisotropy parameter.[29] The availability of good-quality TOF distributions at a large number of polarization angles allowed us to determine *β as a function of the kinetic energy*.[30-32] As shown in Figure 6, the intensities and shapes of the TOF spectra measured with $\Theta = 15°$ exhibit a considerable polarization dependence which is due to the highly anisotropic recoil combined with the fact that the TOF distribution at a given laser polarization angle ϵ spans a wide range of CM angles θ (see the Newton diagram on top of Figure 6). A set of TOF distributions measured at 10 different polarization angles was analyzed according to the procedure described by Frey and Felder.[32] For every flight time channel t, the signal $N(\epsilon;t)$ as a function of ϵ was fitted to the analytical form

$$N(\epsilon;t) = N_{iso}(t)\{1 + \beta(t)P_2(cos(\theta(\epsilon;t) - \theta_0(t)))\} \quad (1)$$

where the fitting parameters $N_{iso}(t)$, $\beta(t)$, and $\theta_0(t)$ represent the isotropic TOF signal, anisotropy parameter, and angular offset angle, respectively.[32] As illustrated by the Newton diagram in Figure 6, the CM angle θ depends both on the polarization angle ϵ and on the photofragment flight time t. Taking into account the kinematic averaging effects and the incomplete laser polarization, the anisotropy distribution $\beta(t)$ displayed in Figure 7a was obtained. A drop from $\beta \sim 1.7$ to $\beta \sim 1.5$ is evident in the flight time region near 160 μs, i.e. between the first two

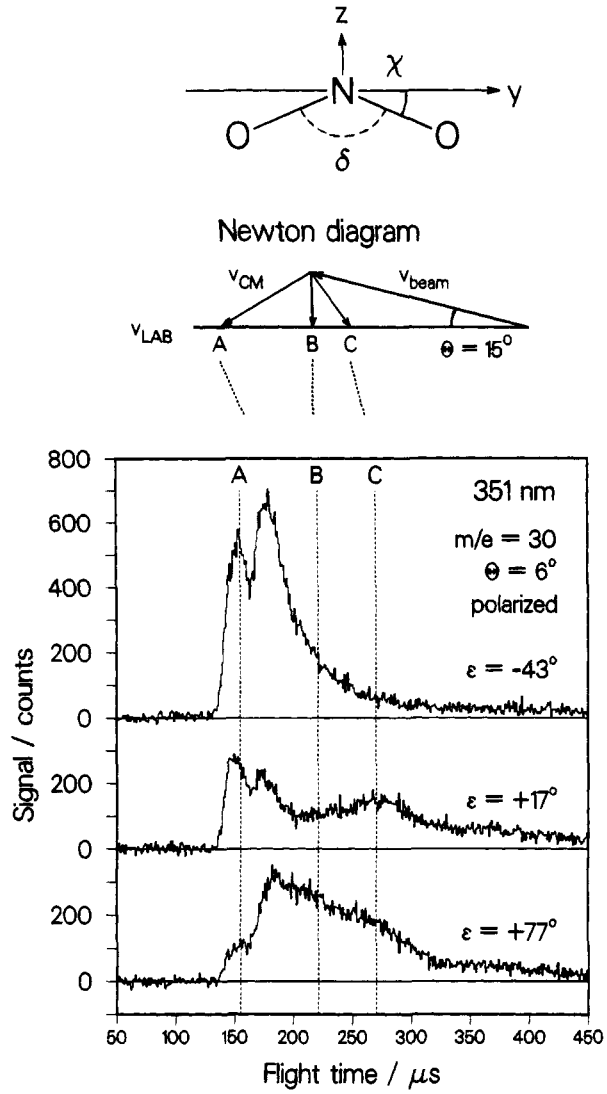

Figure 6. Photodissociation of NO_2 at 351 nm. Polarized TOF distributions of the NO fragment ($m/e = 30$) measured with the LAB angle $\Theta = 15°$ and three different polarization angles ϵ. The geometry of the parent molecule and the Newton diagram of the dissociation kinematics are shown in the top panels.

TOF peaks (cf. the spectrum shown in Figure 7c). The adequacy of our analysis is demonstrated in Figure 7b, where the offset angle θ_0 is also plotted vs the flight time. This angle should be zero if the angular distribution $w(\theta)$ is appropriately transformed from the LAB to the CM system, and indeed, θ_0 is very close to zero except in the region denoted by the dashed vertical line which represents the nominal transition between forward and backward scattered fragments. Since the LAB to CM transformation is rather ill-defined in this region, we can safely attribute the residual angular offset to experimental inaccuracies. Similar to the data recorded at 351 nm, a set of eight polarized TOF distributions was obtained at 355 nm and analyzed as described above.

The anisotropy parameter plotted as a function of total translational energy is shown in Figures 8a (355 nm) and 9a (351 nm). Again, a steplike behavior of β is found in the translational energy region near the threshold for the NO(v=1) formation. This leads us to assign a constant β value to each vibrational channel; that is, we average $\beta(E_T)$ over the kinetic regions pertaining to the formation of NO(v=0) and NO(v=1). Because of experimental uncertainties, the anisotropy at $E_T <$ 800 cm^{-1} is extrapolated from the higher-energy region as shown in Figures 8a and 9a. The pertinent results are collected

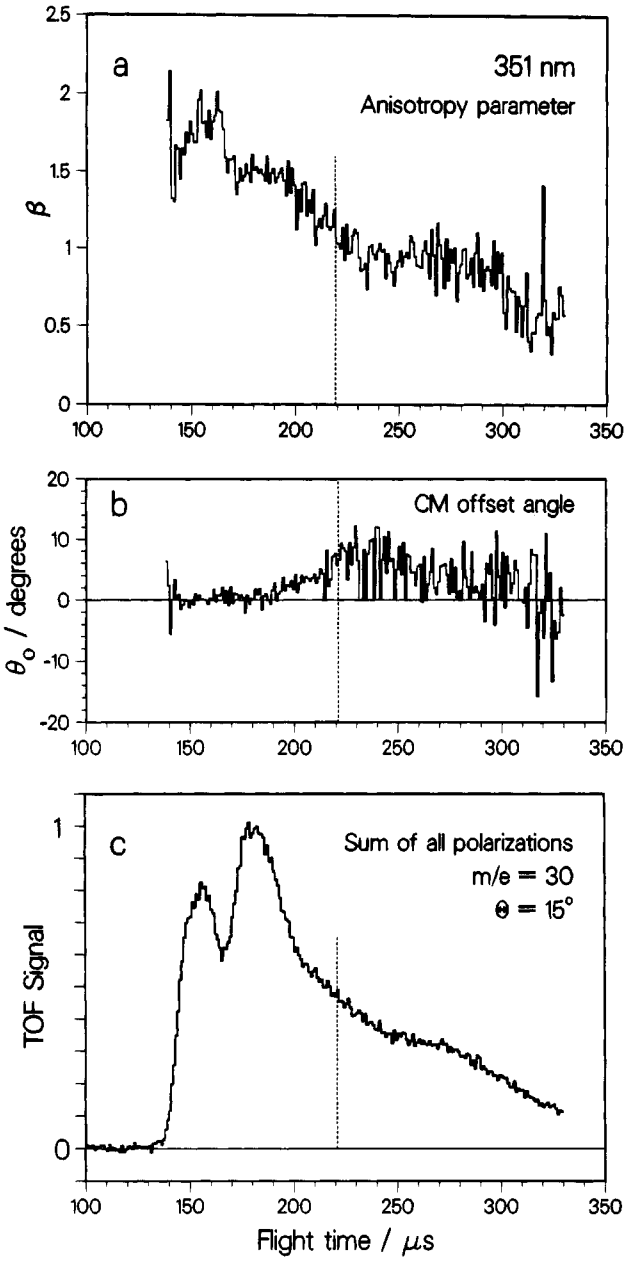

Figure 7. Photodissociation of NO_2 at 351 nm: (a) anisotropy parameter β and (b) offset angle θ_0 derived by fitting the polarized TOF data of Figure 6 to eq 1 in the text. The unpolarized TOF signal (c) is shown for comparison.

TABLE 1: Summary of the Present Experimental Results

wavelength (nm)	355	355	351	351
NO vib state	$v = 0$	$v = 1$	$v = 0$	$v = 1$
E_{avl} (cm^{-1})	3038	1162	3359	1483
$\langle\beta\rangle$	1.42 ± 0.03	1.25 ± 0.02	1.77 ± 0.1	1.48 ± 0.1
$\langle A_0^{(2)}\rangle$	-0.39 ± 0.02	-0.35 ± 0.03	-0.39 ± 0.02	-0.36 ± 0.03
% population	62 ± 3	38 ∓ 3	57 ± 3	43 ∓ 3

in Table 1. It should be noted that while at 355 nm the main uncertainty in the averaged β values arises from the statistical counting error of the TOF signals, there is at 351 nm an additional systematic uncertainty related to the correction for the incomplete laser polarization. The error limits given in Table 1 were calculated by taking into account an error of ±1% for the degree of laser polarization.

We now return to the translational energy distributions. In principle, $P(E_T)$ could be determined by applying the standard forward convolution method[27,28] to the isotropic TOF signal $N_{iso}(t)$ derived from the least-squares fit of the polarized TOF data

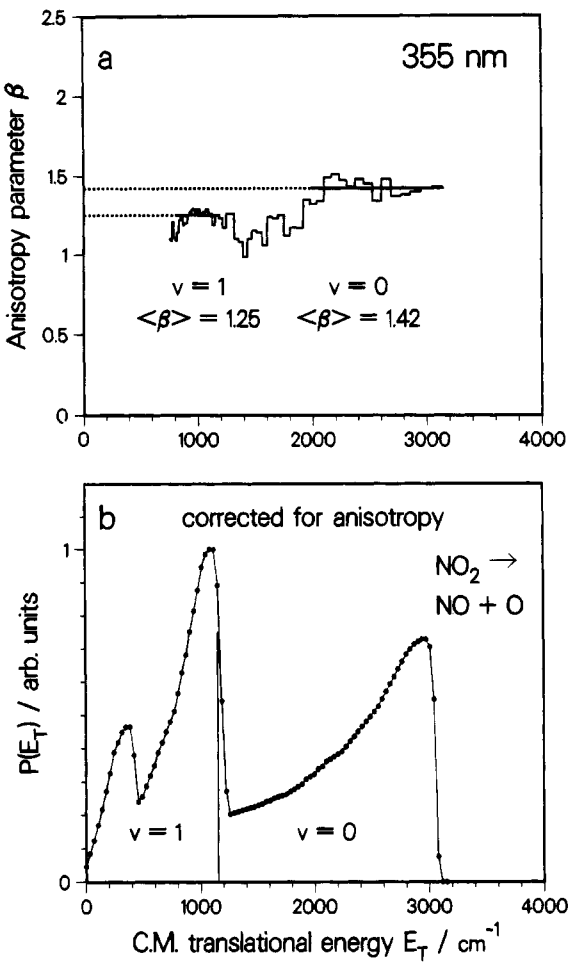

Figure 8. Photodissociation of NO_2 at 355 nm. (a) Anisotropy parameter β vs total translational energy. The horizontal solid lines denote the averaged β values pertaining to the formation of NO(v=0) and NO(v=1). (b) Isotropic $P(E_T)$ derived by rescaling the distribution of Figure 5a with the angular normalization factor $8/(4 + \langle\beta\rangle)$.

according to eq 1. In practice, however, the $N_{iso}(t)$ signal is very noisy. Therefore, in view of the large set of available *unpolarized* TOF data, we adopted a different approach. As detailed e.g. in ref 31 the apparent $P(E_T)$ derived from unpolarized TOF data can be transformed to the true isotropic distribution by rescaling the probability $P(E_T)$ with the factor $8/(4 + \beta(t))$, which results from the integration of $w(\theta)$ in the plane perpendicular to the laser propagation axis. To overcome the statistical fluctuations of $\beta(E_T)$, the correction of $P(E_T)$ was accomplished by inserting the *averaged* anisotropy parameters listed in Table 1. This procedure yielded the corrected, isotropic $P(E_T)$ distributions displayed in Figures 8b and 9b. While the partitioning into the contributions from the product vibrational states NO(v=0) and NO(v=1) will be discussed in the next section, we can already provide an *upper limit* for the relative population of $v = 1$. The energy balance for the photodissociation of NO_2 in a cold molecular beam is given by

$$E_{avl} = h\nu - D_0 = E_{int}(NO) + E_{int}(O) + E_T \qquad (2)$$

where E_{avl} is the available energy to be distributed among the photofragments, $h\nu$ is the photon energy, and $D_0 = 25\,130 \pm 2$ cm^{-1} is the dissociation energy of the parent molecule.[2,3] By virtue of (2), the total translational energy distribution $P(E_T)$ is directly related to the distribution of the internal energy E_{int} of the fragment *pairs*. Moreover, because the O atom can only be formed in the three sublevels $^3P_{J=2,1,0}$, the value of $E_{int}(O)$ is restricted to be either 0, 158.5, or 226.5 cm^{-1}.[33] Accordingly,

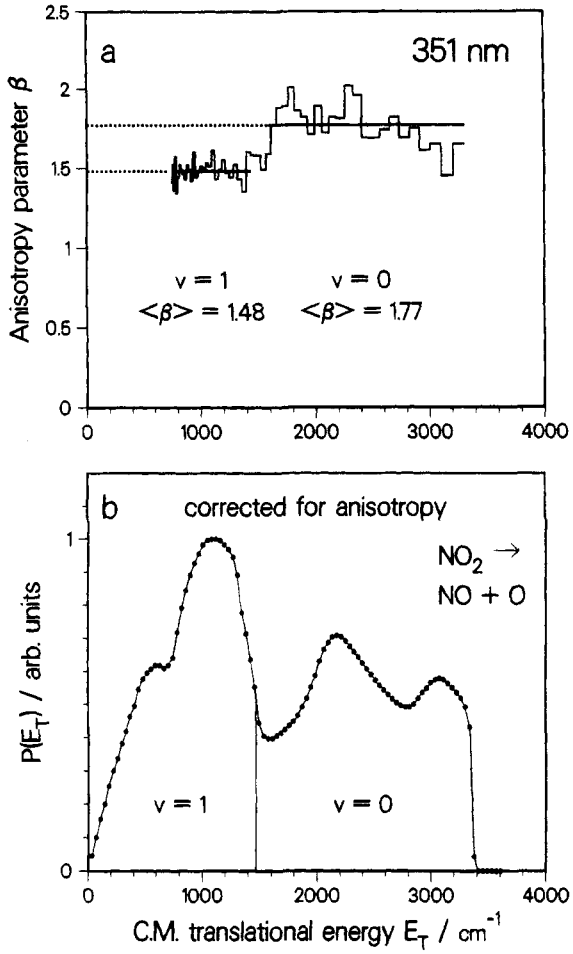

Figure 9. Photodissociation of NO_2 at 351 nm. (a) Anisotropy parameter β vs total translational energy. The horizontal solid lines denote the averaged β values pertaining to the formation of NO(v=0) and NO(v=1). (b) Isotropic $P(E_T)$ derived by rescaling the distribution of Figure 5b with the angular normalization factor $8/(4 + \langle\beta\rangle)$.

the $P(E_T)$ distribution essentially reflects the internal energy distribution of the NO fragment. Inserting the vibrational energy $E_{int}(NO_{v=1}) = 1876$ cm^{-1},[34] we find that any NO product formed with $E_T > 1162$ cm^{-1} at 355 nm, or with $E_T > 1483$ cm^{-1} at 351 nm, is necessarily in $v = 0$. From the integration of the pertinent energy regions of the $P(E_T)$ distributions given in Figures 8b and 9b, we conclude that the populations of NO(v=1) produced at 355 and 351 nm cannot exceed 42% and 50%, respectively. These values are *upper limits* for the populations and are subject to an uncertainty of ±2% caused by the finite kinetic energy resolution of our apparatus. We further note that NO(v=2) is not accessible at the photon energies used in this work. As will be discussed in the next section, absolute values of the population of NO(v=1) can be obtained by taking into account the rotational distributions determined by LIF spectroscopy.

3.2. LIF Measurements. Following excitation with linearly polarized light at the wavelength 355 and 351 nm, the population of the emerging NO photofragments in the individual rotational states were measured with 2 + 1 photon LIF at $\theta(\vec{e}_d,\vec{e}_p) = 0°$ and 90°. With these measurements the rotational alignment $A_0^{(2)}$ for various J states in $v = 0$ and $v = 1$ was determined according to published procedures.[25] Care was taken to use only single rotationally resolved lines, which is of particular importance for the ground vibrational state of NO where parts of the rotationally resolved spectrum overlap with the 1−1 transition.

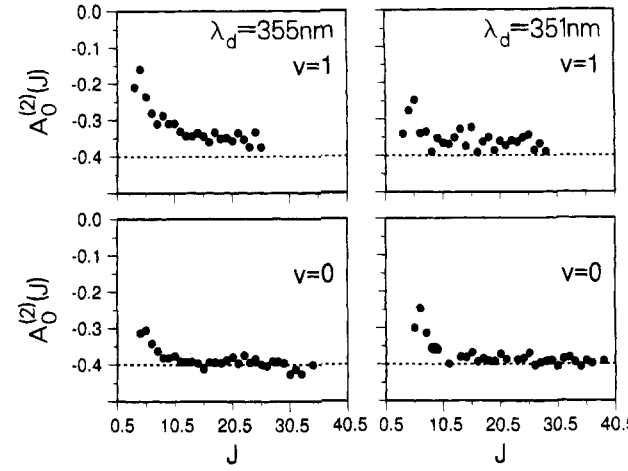

Figure 10. Photodissociation of NO_2 at 355 and 351 nm. Rotational alignment $A_0^{(2)}$ vs angular momentum quantum number J of the NO(v=0,1) fragment obtained from LIF data.

Figure 10 shows the combined rotational alignment values of all substates ($^2\Pi_{\pm1/2}$, $^2\Pi_{\pm2/3}$) as a function of the quantum number J for the two populated vibrational states at the dissociation wavelengths 355 and 351 nm. Except for the depolarization effect at low J values[35,36] (here between $J = 0.5$ and ~10.5), $A_0^{(2)}$ is essentially independent of J. The average value $\langle A_0^{(2)}\rangle$ was found to be −0.39 ± 0.02 ($v = 0$) and −0.35 ± 0.03 ($v = 1$) at 355 nm and −0.39 ± 0.02 ($v = 0$) and −0.36 ± 0.03 ($v = 1$) at 351 nm. All four values are close to the high-J limiting value of −0.4, which corresponds to a dipole transition moment $\vec{\mu}$ perpendicular to $\vec{J}$.

The rotational distributions of NO(v=0,1) measured by LIF were found to be very similar to those already reported by other groups.[3,4,14] On the basis of this result we were able to determine the absolute values for the NO vibrational distributions obtained from the TOF measurements. The relative populations of NO(v=0) with rotational quantum number $N \geq 32$ are 7 ± 3% at 355 nm and 12 ± 3% at 351 nm. These fractions represent the photofragments NO(v=0) having a kinetic energy smaller than the threshold of NO(v=1) and hence appearing in a region of the TOF spectrum overlapping with the signal of NO(v=1). Including this correction to the integrated segments of the $P(E_T)$ distributions reduces the population of $v = 1$ from 42% to 38% at 355 nm and from 50% to 43% at 351 nm (cf. Table 1).

4. Discussion

As has been amply discussed in the literature,[37] the absorption spectrum of NO_2 in the region of interest for the present study is highly complex owing to the strong vibronic coupling between the excited electronic state $^2B_2$ and the ground state $^2A_1$, with the possible participation of the two other low-lying electronic states $^2A_2$ and $^2B_1$. In spite of the spectral simplification achieved by using a cold supersonic beam, many of the apparently single rovibronic bands in the absorption spectrum actually consist of overlapping resonances.[3] PHOFRY spectra for selected rotational quantum states of the NO product[3,17] show a considerable state dependence, which in turn implies that the product state distribution of NO is critically dependent on the photoexcitation step. The fact that a slight change in the photolysis wavelength can lead to a significant change of the rotational distribution might seem to preclude a detailed interpretation of the present results, since these were obtained at the fixed and somewhat arbitrary wavelengths provided by our nontunable photolysis lasers. Moreover, in the case of the

XeF excimer laser, three main emission bands at 349, 351, and 353 nm, with 351 nm being the most intense line, lead to the incoherent excitation of several transitions. In spite of these complications, however, a comparative investigation by means of PTS and LIF can help to clarify some important issues concerning the photodissociation dynamics of NO_2.

First, we briefly address the photodissociation rate constant $k(E)$. In recent femtosecond beam experiments Wittig and coworkers[5] found an increasing dissociation rate from the threshold up to about 1000 cm^{-1} excess energy, where $k(E)$ becomes $\sim 3 \times 10^{12}$ s^{-1}. A substantially greater value is therefore expected for the present experiments which involve excess energies >3000 cm^{-1}. We now turn our attention to the vector correlations β and $A_0^{(2)}$ of this subpicosecond process. Although explicit quantum mechanical expressions have been derived both for β[38,39] and for $A_0^{(2)}$[40] in a triatomic system, we first consider a simple classical mechanical model in order to discuss the main features of our experimental results. As has been detailed elsewhere,[7,29,41,42] the anisotropy parameter can be written as

$$\beta = 2P_2(\cos\chi)\frac{1+\omega^2\tau^2}{1+4\omega^2\tau^2} \tag{3}$$

where χ denotes the effective angle between the electronic transition moment $\vec{\mu}$ and the final recoil velocity $\vec{v}$ in the CM system, ω is the angular frequency of the parent rotation, and $\tau = k^{-1}$ is the average lifetime of the excited molecule. The first factor on the right-hand side of (3) accounts for the dissociation geometry whereas the second factor describes the anisotropy loss caused by the rotational reorientation of the dissociation complex. In our mechanical model of the NO_2 dissociation the angular momentum $\vec{J}$ of the NO fragment is perpendicular to the molecular plane; i.e., $\vec{J}$ is parallel to the x axis in the corotating molecular frame (see Figure 6). The rotational alignment is then given by

$$A_0^{(2)} = \frac{4}{5}P_2(\cos\gamma)\frac{1+\omega^2\tau^2}{1+4\omega^2\tau^2} \tag{4}$$

where γ is the angle between the transition moment $\vec{\mu}$ and the x axis.

On the basis of a detailed study of the rotational temperature T_r of pulsed supersonic beams of NO_2 seeded in He by Robra,[43] we expect that under the expansion conditions used in our LIF experiments $T_r \sim 7$ K. The corresponding average rotational frequency is $\omega \sim 5 \times 10^{11}$ s^{-1} and, accordingly, $\omega\tau < 0.1$. This implies that both β and $A_0^{(2)}$ are close to their limiting values for instantaneous dissociation ($\omega\tau \to 0$) and, hence, reflect almost exclusively the geometry-dependent terms in (3) and (4). Since the alignment parameter measured for NO(v=0) at both photolysis wavelengths converges for high J values to $A_0^{(2)} = -0.39 \pm 0.02$, in good agreement with the previously reported value of -0.35 ± 0.05 for NO(v=1) at 355 nm,[14] we conclude that $\vec{\mu}$ is polarized either in the y or z direction and that $\omega\tau$ is indeed very small. Moreover, since the large and positive β parameters (see Table 1) are incompatible with a transition moment in the z direction, $\vec{\mu}$ must be oriented along the y direction, i.e., parallel to the line connecting the two O atoms (see Figure 6). This is in accordance with a $^2B_2 \leftarrow {}^2A_1$ electronic transition. Based on our alignment measurements, the other symmetry-allowed transition in this energy region, $^2B_1 \leftarrow {}^2A_1$, contributes less than 3% of the absorption at the photolysis wavelengths studied.

Returning to the β parameter, we note that a wide range of values has previously been reported by various investigators.[7,11,12] This can be rationalized by the different rotational temperatures used in these studies. Given the lifetime and rotational constants of NO_2, an increase from $T_r = 7$ K (this work) to 370 K (ref 7) raises the value of $\omega\tau$ from <0.1 to >7 which, according to eq 3, implies a substantial loss of anisotropy. Once this fact is taken into account, the β parameters obtained so far are in reasonable agreement with each other. However, a closer inspection of β at a given rotational temperature as a function of photolysis wavelength or vibrational energy of the NO fragment reveals significant trends. In their early PTS investigation at 347 nm, Busch and Wilson[7] found $\beta(v$=0) = 0.74 and $\beta(v$=1) = 0.46. While these authors mentioned the possibility of "separate dynamics" as the cause of the different anisotropies in the two dissociation channels, they clearly recognized that under their experimental conditions a different effect was responsible for the observed variation of β. With an effusive beam at T = 370 K the large *tangential* velocity caused by the parent rotation leads to a deviation from axial fragment recoil. This deviation is greater for the slowly recoiling fragments in the channel producting NO(v=1), and hence, the corresponding anisotropy parameter experiences a stronger depolarization. In contrast, under our supersonic jet conditions, the rotational frequency is sufficiently small to render nonaxial recoil a negligible cause of anisotropy loss. Moreover, the high kinetic energy resolution of our apparatus allows us to distinguish the steplike behavior of β as a function of product vibrational state (see Figures 8a and 9a) as opposed to a continuous variation of β as a function of recoil velocity, which would be expected if nonaxial recoil were the cause of anisotropy loss.

In the classical model adopted so far, the dependence of β on the vibrational state of NO must be attributed to a geometrical effect. More specifically, neglecting the near-unity lifetime factor in eq 3, the observed β values are related to the effective recoil angle χ, which in turn is related to the average O–N–O bond angle in the excited molecule according to $\delta = 180° - 2\chi$, as illustrated in Figure 6. Our results would indicate that the bond angle is strongly dependent on the photodissociation channel, ranging from $\delta = 148°$ in the case of NO(v=0) formation at 351 nm to $\delta = 120°$ in the case of NO(v=1) produced at 355 nm. For comparison, the equilibrium angle of NO_2 in the electronic ground state is $\delta = 134°$.[44] However, the explicit connection between the effective recoil angle χ, which is an asymptotic property of the dissociation process, and the evolution of the bond angle in the course of the dissociation process is by no means obvious. Moreover, the classical description of the dissociation may well be inadequate. The low rotational temperature of our jet-cooled sample, the presence of interacting electronic states, and the observation of fluctuations in the product distributions[3,4,14,17] strongly suggest that quantum effects play an important role in the decay process. Under such conditions the anisotropy parameter assumes a complicated form that depends on the details of the excitation process and the potential energy surface, as well as on the product quantum state being probed.[38,39,45] Indeed, our observation that at both photolysis wavelengths the rotational alignment $A_0^{(2)}$ of NO(v=1) is slightly but significantly reduced points to the presence of subtle effects that are not explicable with simple geometrical arguments in a classical model. A clarification of these issues will thus require accurate quantum dynamics calculations based on high-quality potential energy surfaces. Such calculations may also reveal a dependence of β on the product *rotational* state which, however, is not presently resolvable with our PTS apparatus.

TABLE 2: Vibrational Distribution of the NO Fragment

wavelength nm	E_{avl}[a]	$P(v=1)$[b]	method	ref
369.3	1949	27	LIF	4
	1998	20		
	2061	20		
	2200	42		
	2700	44		
355	3038	41 ± 6	LIF	4
		38 ± 3	PTS	this work
351	3359	63 ± 7	LIF	2
		43 ± 3	PTS	this work
347	3679	~50	PTS	6

[a] Available energy in cm^{-1} units. [b] Relative vibrational population in percent.

The vibrational distribution of the NO fragment has been the subject of considerable debate. This interest is mainly due to the fact that NO_2 is a "benchmark" molecule for the test of statistical models applying to the dissociation of molecules without barrier in the exit channel.[16] As already mentioned in the Introduction, the vibrational distribution obtained at 347 nm by Busch and Wilson[7] has served as evidence for the adequacy of statistical models such as the statistical adiabatic channel model.[8] In their recent LIF study, Reisler and co-workers[4] determined the vibrational distribution for a wide range of photolysis wavelengths between 369.3 and 355 nm, corresponding to an excess energy range between 1949 and 3038 cm^{-1} (see Table 2). While the population of NO(v=1) does not increase monotonically as a function of the excess energy, and even *decreases* when E_{avl} is raised from 1949 to 1998 cm^{-1}, the population in $v = 1$ is always well below 50%. In contrast, at only slightly higher photon energy, Welge and co-workers found an inverted vibrational distribution, with 63% in $v = 1$ at 351 nm.[2] Our experiments carried out at 355 and 351 nm bridge the gap in excess energy of the two investigations mentioned above. As discussed in the previous section, application of the energy balance (3) allowed us to determine reliable *upper limits* of the population in $v = 1$. The actual populations in $v = 1$ given in Tables 1 and 2 were then obtained by incorporating the LIF results in order to correct the TOF data for the overlap of the $v = 0$ and $v = 1$ signals. Our findings conclusively show that the vibrational distribution of NO produced at 355 and 351 nm is *not* inverted. This agrees with the result at 355 nm of Reisler and co-workers[4] but disagrees with the result at 351 nm reported earlier.[2] Moreover, we can state that the photodissociation of NO_2 with excess energies up to ~3400 cm^{-1} produces NO fragments with a vibrational distribution that is consistent with the predictions of state-of-the-art statistical calculations.[16]

Finally, we address the rotational distribution of the NO product. Since this is known to be a sensitive and fluctuating function of the photolysis wavelength,[3,4,14,17] great care is needed when comparing the results of various experiments. Indeed, due to the limited translational energy resolution and the nonlinear relation between the rotational quantum number and the translational energy, no attempt was made to derive accurate shapes of the rotational distributions from the TOF data. Clearly, however, the complex shape of the TOF signals shows that the underlying rotational distributions have a bimodal, perhaps even a multimodal, shape. This is the case both with the multiline emission of the XeF laser at 351 nm, as reported by Robra *et al.*,[2] and also with the narrow-band Nd:YAG laser at 355 nm, as found by Hradil *et al.*[11] and Changlong *et al.*[14] and in the present work. Since the bandwidth of the latter (<2 cm^{-1}) is narrower than the line width of the lifetime broadened spectral features of NO_2 (>25 cm^{-1}), the distinct bimodal rotational distribution of NO(v=1) produced at 355 nm (see Figure 8b) is unlikely to be due to incoherent excitation of several transitions. Thus, based on the bi- or multimodal nature of the rotational distributions, which is apparent even with the energy resolution of our PTS apparatus, the dynamics of the rotational degrees of freedom cannot be considered to be statistical.

5. Conclusion

In the energy region about 3400 cm^{-1} above the dissociation threshold, laser excitation of NO_2 prepares eigenstates which are strongly mixed rovibronic states of the electronic states $^2B_2$ and $^2A_1$ with dominant $^2A_1$ ground state character. The highly excited $^2A_1$ vibronic states involved in the coupling are well above the onset of vibronic chaos.[46] Laser excitation of such mixed eigenstates, which are furthermore embedded in a continuum, is bound to favor the dynamics of statistical (unimolecular) processes. The continuum is that of the ground state $^2A_1$ of NO_2 which gives rise to the formation of the fragments NO($X^2\Pi_{\Omega=1/2,3/2}$) and O($^3P_{J=2,1,0}$) without a potential barrier and hence without a well-defined transition state. In spite of the subpicosecond lifetime of the excited complex, this delocalized excitation yields a vibrational state distribution in NO which is close to the one predicted years ago by Quack and Troe[8] using the statistical adiabatic channel model but subsequently questioned by experimental findings. The recently reported vibrational distributions by Reisler and co-workers[4] coincide at 3038 cm^{-1} with the present experimental results corroborating their findings which were obtained from LIF measurements by integrating the rotational state distributions in the NO(v=0,1) fragments. A nonstatistical decay dynamics is, however, indicated for the rotational degrees of freedom as manifested by bimodal (or multimodal) rotational distributions of NO(v=0,1).

The anisotropy parameter β approaches values as high as 1.8. This result and the various lower values reported earlier can be reconciled when the different parent rotational temperatures are taken into account.[7,11,12] The high β value is accompanied by an alignment parameter close to the minimum value ($A_0^{(2)} = -0.4$), indicating that essentially no loss of initial anisotropy occurs prior to dissociation which is consistent with a subpicosecond dissociation time. Furthermore, β was found to be independent of the fragment recoil velocity but to change with the vibrational level of NO. The dynamics leading to NO(v=0) and NO(v=1) are apparently different; *i.e.*, the initially prepared superposition of the rovibronic state and the continuum state (the continuum eigenstate) evolves differently in time toward the product states $v = 0$ and $v = 1$, as manifested in the vector property β. This result also indicates that the classical model for extraction of upper-limit dissociation lifetimes from β[42] is not applicable in the present case where quantum mechanical effects (interferences) appear to play an important role in the decay process.

Acknowledgment. Support by the Schweizerischer Nationalfonds zur Förderung der wissenschaftlichen Forschung and by the Alfred Werner Legat is gratefully acknowledged. The authors thank PD Dr. R. Schinke and Profs. H. Reisler, M. Quack, and M. Shapiro for stimulating discussions, Dr. P. R. Willmott for critically reading the manuscript, and Mr. R. Pfister for the preparation of NO_2 samples.

References and Notes

(1) Jackson, W. M.; Okabe, H. *Adv. Photochem.* **1986**, *13*, 17.
(2) Robra, U.; Zacharias, H.; Welge, K. H. *Z. Phys. D* **1990**, *16*, 175.

(3) Reid, S. A.; Robie, D. C.; Reisler, H. *J. Chem. Phys.* **1994**, *100*, 4256.
(4) Hunter, M.; Reid, S. A.; Robie, D. C.; Reisler, H. *J. Chem. Phys.* **1993**, *99*, 1093.
(5) (a) Ionov, S. I.; Brucker, G. A.; Jaques, C.; Chen, Y.; Wittig, C. *J. Chem. Phys.* **1993**, *99*, 3420. (b) Wittig, C.; Ionov, S. I. *J. Chem. Phys.* **1994**, *100*, 4714.
(6) Busch, G. E.; Wilson, K. R. *J. Chem. Phys.* **1972**, *56*, 3626.
(7) Busch, G. E.; Wilson, K. R. *J. Chem. Phys.* **1972**, *56*, 3638.
(8) Quack, M.; Troe, J. *Ber. Bunsen-Ges. Phys. Chem.* **1975**, *79*, 469.
(9) Zacharias, H.; Geilhaupt, M.; Meier, K.; Welge, K. H. *J. Chem. Phys.* **1981**, *74*, 218.
(10) Zacharias, H.; Meier, K.; Welge, K. H. In *Energy Storage and Redistribution in Molecules*; Hinze, J., Ed.; Plenum Press: New York, 1983; p 107.
(11) (a) Suzuki, T.; Hradil, V. P.; Hewitt, S. A.; Houston, P. L.; Whitaker, B. J. *Chem. Phys. Lett.* **1991**, *187*, 257. (b) Hradil, V. P.; Suzuki, T.; Hewitt, S. A.; Houston, P. L.; Whitaker, B. J. *J. Phys. Chem.* **1993**, *99*, 4455.
(12) Mons, M.; Dimicoli, I. *J. Chem. Phys.* **1989**, *90*, 4037.
(13) Butenhoff, T. J.; Rohlfing, E. A. *J. Chem. Phys.* **1993**, *98*, 5469.
(14) Changlong, N.; Hua, L.; Pfab, J. *J. Phys. Chem.* **1993**, *97*, 7458.
(15) Brucker, G. A.; Ionov, S. I.; Chen, Y.; Wittig, C. *Chem. Phys. Lett.* **1992**, *194*, 301.
(16) Klippenstein, S. J.; Radivoyevitch, T. *J. Chem. Phys.* **1993**, *99*, 3644.
(17) (a) Miyawaki, J.; Yamanouchi, K.; Tsuchiya, S. *J. Chem. Phys.* **1993**, *99*, 254. (b) Miyawaki, J.; Yamanouchi, K.; Tsuchiya, S. *J. Chem. Phys.* **1994**, *100*, 4716.
(18) Wodtke, A. M.; Lee, Y. T. In *Molecular Photodissociation Dynamics*; Ashfold, M. N. R., Baggott, J. E., Eds.; Royal Society of Chemistry: London, 1987; p 31.
(19) Ashfold, M. N. R.; Lambert, I. R.; Mordaunt, D. H.; Morley, G. P. *J. Phys. Chem.* **1992**, *96*, 2938.
(20) (a) Felder, P. *Chimia* **1993**, *48*, 43. (b) Felder, P.; Yang, X.; Baum, G.; Huber, J. R. *Isr. J. Chem.* **1994**, *34*, 33.
(21) Felder, P. *Chem. Phys.* **1990**, *143*, 141.
(22) Thelen, M.-A.; Felder, P.; Huber, J. R. *Chem. Phys. Lett.* **1993**, *213*, 275.
(23) Minton, T. K.; Felder, P.; Brudzynski, R. J.; Lee, Y. T. *J. Chem. Phys.* **1984**, *81*, 1759.
(24) Kades, E.; Rösslein, M.; Brühlmann, U.; Huber, J. R. *J. Phys. Chem.* **1993**, *97*, 989.
(25) Dubs, M.; Brühlmann, U.; Huber, J. R. *J. Chem. Phys.* **1986**, *84*, 3106.
(26) Harrison, J. A. To be published.
(27) Sparks, R. K.; Shobatake, K.; Carlson, L. R.; Lee, Y. T. *J. Chem. Phys.* **1981**, *75*, 3838.
(28) Frey, J. G. *Mol. Phys.* **1993**, *79*, 1287.
(29) Zare, R. N. *Mol. Photochem.* **1972**, *4*, 1.
(30) Haas, B.-M.; Felder, P.; Huber, J. R. *Chem. Phys. Lett.* **1991**, *180*, 293.
(31) Felder, P. *Chem. Phys.* **1991**, *155*, 435.
(32) Frey, J. G.; Felder, P. *Mol. Phys.* **1992**, *75*, 1419.
(33) *JANAF Thermochemical Tables*; *J. Phys. Chem. Ref. Data* **1985**, *14* (Suppl. 1).
(34) Herzberg, G. *Molecular Spectra and Molecular Structure*; Krieger: Malabar, 1989; Vol. 1.
(35) Andresen, P.; Ondrey, G. S.; Titze, B.; Rothe, E. W. *J. Chem. Phys.* **1984**, *80*, 2548.
(36) Greene, C. H.; Zare, R. N. *J. Chem. Phys.* **1983**, *78*, 6741.
(37) See e.g. the articles quoted in refs 3 and 5a.
(38) Balint-Kurti, G. G.; Shapiro, M. *Chem. Phys.* **1981**, *61*, 137.
(39) Singer, S. J.; Freed, K. F.; Band, Y. *J. Chem. Phys.* **1983**, *79*, 6060.
(40) Nagata, T.; Kondow, T.; Kuchitsu, K.; Loge, G. W.; Zare, R. N. *Mol. Phys.* **1983**, *50*, 49.
(41) Jonah, C. *J. Chem. Phys.* **1971**, *55*, 1915.
(42) Yang, S.; Bersohn, R. *J. Chem. Phys.* **1974**, *61*, 4400.
(43) Robra, U. Ph.D. Thesis, Universität Bielefeld, 1984.
(44) Bird, G. R.; Baird, J. C.; Jache, A. W.; Hodgeson, J. A.; Curl, Jr. R. F.; Kunkle, A. C.; Bransford, J. W.; Rastrup-Andersen, J.; Rosenthal, J. *J. Chem. Phys.* **1964**, *40*, 3378.
(45) Waldeck, J. R.; Shapiro, M.; Bersohn, R. *J. Chem. Phys.* **1993**, *99*, 5924.
(46) (a) Delon, A.; Jost, R. *J. Chem. Phys.* **1991**, *95*, 5686. (b) Delon, A.; Jost, R.; Lombardi, M. *J. Chem. Phys.* **1991**, *95*, 5701.